

Available online at www.sciencedirect.com

ScienceDirect

journal homepage: www.elsevier.com/locate/ije

Effect of single-cation doping and codoping with Mn and Fe on the photocatalytic performance of TiO₂ thin films

M.Z. Lin^a, H. Chen^a, W.F. Chen^a, A. Nakaruk^b, P. Koshy^a, C.C. Sorrell^{a,*}

^aSchool of Materials Science and Engineering, University of New South Wales, Sydney, NSW 2052, Australia

^bDepartment of Industrial Engineering, Faculty of Engineering, Naresuan University, Phitsanulok 65000, Thailand

ARTICLE INFO

Article history:

Received 8 November 2013

Received in revised form

13 January 2014

Accepted 3 February 2014

Available online 14 May 2014

Keywords:

Titanium dioxide

Mn-doping

Fe-doping

Codoping

Photocatalysis

ABSTRACT

TiO₂ thin films with varying Mn and Fe dopant levels (0.01–5.00 mol% metal basis; single cation doping and codoping) were deposited on soda-lime-silica glass substrates by spin coating, followed by annealing in air at 450 °C for 2 h. The mineralogical, morphological, optical, and photocatalytic properties of the thin films were determined. The fabricated films were ~250 nm thick and they were comprised of grains of ~20–30 nm size. Anatase (or amorphous titania) was the only phase in essentially all the films, with the dopants' being soluble in anatase. All of the films were transparent (~80%) in the visible region and the optical indirect band gaps were ~3.4 eV. Photocatalytic testing (≤24 h) showed that the extent of photodegradation decreased with increasing dopant levels. The 0.01 mol% Fe-doped sample showed the best photoactivity since, at this doping level, the negative effects of electron/hole recombination and lattice distortion probably were minimal.

Copyright © 2014, Hydrogen Energy Publications, LLC. Published by Elsevier Ltd. All rights reserved.

Introduction

During the past decade, titanium dioxide (TiO₂, titania) has been investigated extensively, particularly for its photocatalytic properties since TiO₂ has wide-ranging applications, including self-cleaning and self-sanitizing materials, water purification systems, and photovoltaic cells [1,2]. Notably, the potential use of TiO₂ in solar–electricity conversion can reduce both the reliance on fossil fuels and the associated environmental issues due to CO₂ gas emissions.

Generally, TiO₂ can exist as three crystalline polymorphs, namely anatase, rutile, and brookite. However, these polymorphs show differing photocatalytic behaviors owing to variations in their physical and crystallographic properties.

However, anatase is the most photoactive phase of TiO₂ [3] due to its unique crystallographic structure, which increases electron–hole recombination times. Thus, there is a strong interest in understanding the photocatalytic properties of anatase. In addition, anatase can be used in the form of thin films and these provide additional advantages, such as processing flexibility and lower costs compared to bulk forms.

Several techniques have been used to coat TiO₂ (anatase) thin films on glass substrates and these include sputtering [4], laser ablation [5], sol–gel [6], screen printing [7], dip coating [8], spray pyrolysis [9], and spin coating [10]. The latter is used widely in the fabrication of TiO₂ thin films because it has several advantages, including rapid growth rates, capacity for handling large sample sizes, mass production capability, and high yield rates [11]. On the other hand, anatase is known

* Corresponding author. Tel.: +61 2 9385 4421; fax: +61 2 9385 5956.

E-mail address: C.Sorrell@unsw.edu.au (C.C. Sorrell).

to be a wide band gap (optical indirect band gap ~ 3.2 eV) semiconductor, which means that only a small fraction of solar light, less than 5%, is absorbed [12,13]. Therefore, it is important to reduce the band gap in order to enhance the absorption in the visible-light region (400–800 nm) and hence the photocatalytic performance.

Previous research has shown that metal-ion implantation and doping with metals and nonmetals [14] can enhance the photocatalytic performance of TiO₂ thin films. The metal dopants investigated include Mn [13], Fe [10,15], V [16], Mo [17], and Co [10,13]. Doping with Fe has been shown to increase the electron–hole recombination times, thereby increasing the photocatalytic efficiency [15]. On the other hand, doping with Mn has been shown to cause a remarkable red shift in the absorption edge, leading to the formation of a narrow band gap [13]. Codoping has been gaining interest as a method to improve synergistically the photocatalytic efficiency of TiO₂, and the majority of combinations used has involved a metal ion and a nonmetal ion [18,19]. A very limited number of studies has considered the combined effect of using two transition metals as codopants [20–23].

The present work aims to fabricate TiO₂ thin films with varying amounts of dopants (Mn and/or Fe) on glass substrates using spin coating and to investigate the effects of both single-cation doping and codoping on the mineralogical, morphological, topographical, optical, and photocatalytic properties of spin coated thin films.

Experimental procedure

Thin film fabrication

The sample fabrication method for TiO₂ thin films using spin coating has been applied successfully in previous works [11,24]. The precursors for the coating were prepared using titanium tetra-isopropoxide (TTIP, Reagent Grade, 97 wt%, Sigma–Aldrich) dissolved in isopropanol (Reagent Plus, ≥ 99 wt%, Sigma–Aldrich) at 0.1 M titanium concentration (2.84 g of TTIP was diluted to 100 mL volume with isopropanol). The Mn or Fe dopant concentration was varied from 0.01 mol% to 5.00 mol%, as shown in Table 1, by adding MnCl₂·4H₂O or FeCl₃, respectively (both Reagent Plus, ≥ 99 wt %, Sigma–Aldrich), to the solution. The solutions were mixed by stirring manually in a beaker for 1 min without heating. Spin coating (Laurell WS-65052) was done by rapidly

depositing ~ 0.2 mL (ten drops from a syringe) of solution onto a glass substrate (Shanghai Machinery Import and Export Company, China) spun at 2000 rpm in air. The film was dried by spinning for an additional 15 s and the overall process was repeated six more times (viz., ~ 1.4 mL; seventy drops). Subsequent annealing was carried out in a muffle furnace at 450 °C for 2 h; the heating rates were 0.5 °C/min from room temperature to 200 °C and 1 °C/min from 200 °C to 450 °C; the cooling was done naturally.

Characterisation

The mineralogies of the films were examined using glancing-angle X-ray diffraction (GAXRD, 45 kV, 40 mA, PAN-analytical X'pert Materials Research Diffractometer) and laser Raman microspectroscopy (He–Cd UV laser, excitation source of wavelength 442 nm, Renishaw inVia). The surface compositions of the films were assessed using X-ray photoelectron spectroscopy (XPS, 15.2 kV, 10.8 mA, Thermo Scientific ESCA-LAB250Xi). Atomic force microscopy (AFM, tapping mode, Bruker Dimension Icon SPM) was employed to examine the grain and film surface characteristics of the films. High-resolution images of the films were obtained by field emission gun transmission electron microscopy (FEGTEM, 200 kV accelerating voltage, Philips CM200). Optical transmission spectra of the material in the visible region were obtained using UV–VIS spectrophotometry (PerkinElmer Lambda 35).

Photocatalytic performance

The photocatalytic performance was assessed by photo-bleaching of methylene blue (MB) solution with TiO₂ thin films exposed to UV radiation for up to 24 h. The MB solutions were prepared using methylene blue (M9140, dye content ≥ 82 wt%, Sigma–Aldrich) dissolved in deionized water at 10^{-5} M concentration (0.0032 g of MB were diluted to 1 L volume with deionized water) [25]. The MB solutions then were stirred manually in Pyrex beakers for ~ 5 min without heating. Subsequently, the test specimens were placed in solutions and exposed to 365 nm UV radiation from a UV lamp (8 W, 3UV-38, UVP) for different exposure times. The gap between the UV lamp and the MB solution container was 10 cm. Lastly, the tested solutions were analysed by UV–VIS spectrophotometry to determine the extent of degradation.

Results and discussion

Mineralogical characteristics

The laser Raman microspectra for TiO₂ thin films with varying Mn or Fe single-cation dopant concentrations are shown in Fig. 1(a) and (b), respectively. All of the fabricated films were comprised of anatase (peaks at ~ 144 , 197, 399, 519, and 639 cm⁻¹); peaks for neither rutile nor any phases containing Mn, Fe, or other phases were observed. However, the Raman peak for anatase at ~ 144 cm⁻¹ for Mn- or Fe-doped samples was observed to have shifted to higher wavenumbers compared to that of the undoped sample.

Laser Raman microspectra of the codoped samples (Fig. 1(c)) showed that all of the samples had the anatase

Table 1 – Concentrations of Mn and Fe used as single-cation dopants and codopants.

Fe (mol% metal basis)	Mn (mol% metal basis)						
	0	0.01	0.05	0.30	0.60	1.00	5.00
0	•	•	•	•	•	•	
0.01	•	•					
0.05	•		•				
0.30	•			•			
0.60	•				•		
1.00	•					•	
5.00							•

structure except the 5.00% Mn/5.00% Fe codoped TiO_2 thin film, which was amorphous. The anatase peak at 144 cm^{-1} also shifted to higher wavenumbers in these samples. Since the laser Raman microspectra signal depends on vibrational modes, alteration of the lattice through solid solution formation and associated peak shift are as expected.

Fig. 2(a) and (b) shows GAXRD patterns of the Mn- and Fe-doped TiO_2 thin films with varying single-cation dopant levels. These patterns confirm that all of the films consisted only of anatase and that secondary phases resulting from the doping of Mn or Fe were not present or below the level of detection of the instrument. No significant changes were observed in the positions or intensities of the (101) peak with increasing Mn or Fe dopant concentration, indicating that there is little or no effect on the degree of crystallinity in the case of single-cation dopant additions. On the other hand, the GAXRD patterns of codoped TiO_2 thin films show that the degree of crystallinity decreased with increasing dopant level (Fig. 2(c)). That is, the intensity of the anatase peaks slightly decreased with increasing codopant concentrations. At the highest codoping concentration (5.00% Mn/5.00% Fe), the thin film was amorphous, which suggests that high dopant contents tend to hinder anatase recrystallisation.

The absence of phases, such as rutile, Mn, Fe, or other phases, suggests that Mn and Fe ions were incorporated in the TiO_2 lattice and/or their respective oxides were present at levels below the detection limit of the GAXRD unit [16]. Although the detection level of GAXRD generally is $\sim 1\text{ wt}\%$ (1 mol% Mn or Fe corresponds to 1.17 wt% or 1.15 wt%, respectively), laser Raman microscopy is more

sensitive in the detection of very low levels of secondary phases. Therefore, since only anatase was detected using the latter technique, it is probable that the dopants formed a solid solution in the anatase lattice, regardless of the visible effect on the structure at codoping levels of 5.00 mol% Mn/5.00 mol% Fe.

The incorporation of the cations could have occurred by substitutional and/or interstitial means. Moreover, since the dopant cations have different valences compared to Ti^{4+} , the resultant oxygen levels of what effectively is TiO_{2-x} would be altered through the formation of oxygen vacancies [26]. The crystal radii of Ti^{4+} , Mn^{3+} , Mn^{4+} , Fe^{2+} , and Fe^{3+} in sixfold coordination are 0.0745 nm, 0.0785 nm, 0.0670 nm, 0.0780 nm, and 0.0785 nm, respectively [27]. These data show that the differences in crystal radii between Ti^{4+} and Mn^{3+} , Fe^{2+} , and Fe^{3+} is only $\sim 5\%$ and this would be expected to cause finite expansion of the lattice (Mn^{4+} is expected to cause finite contraction of the lattice). However, since GAXRD peak shifts were not detected in the single cation doped samples, these effects cannot be ascertained.

In contrast, data for the codoped TiO_2 films show decreasing peak intensities (and therefore decreasing crystallinity) with increasing codopant levels and this was noticeable even at total dopant levels $\leq 1.00\text{ mol}\%$. Therefore, codoping and doping at the same overall levels showed different outcomes, which suggests that codoping may have caused clustering of the dopants, thereby amplifying their capacity to distort the lattice [28,29]. Another possibility is that intervalence charge transfer [30] has occurred, which would require close physical association of the dopants and

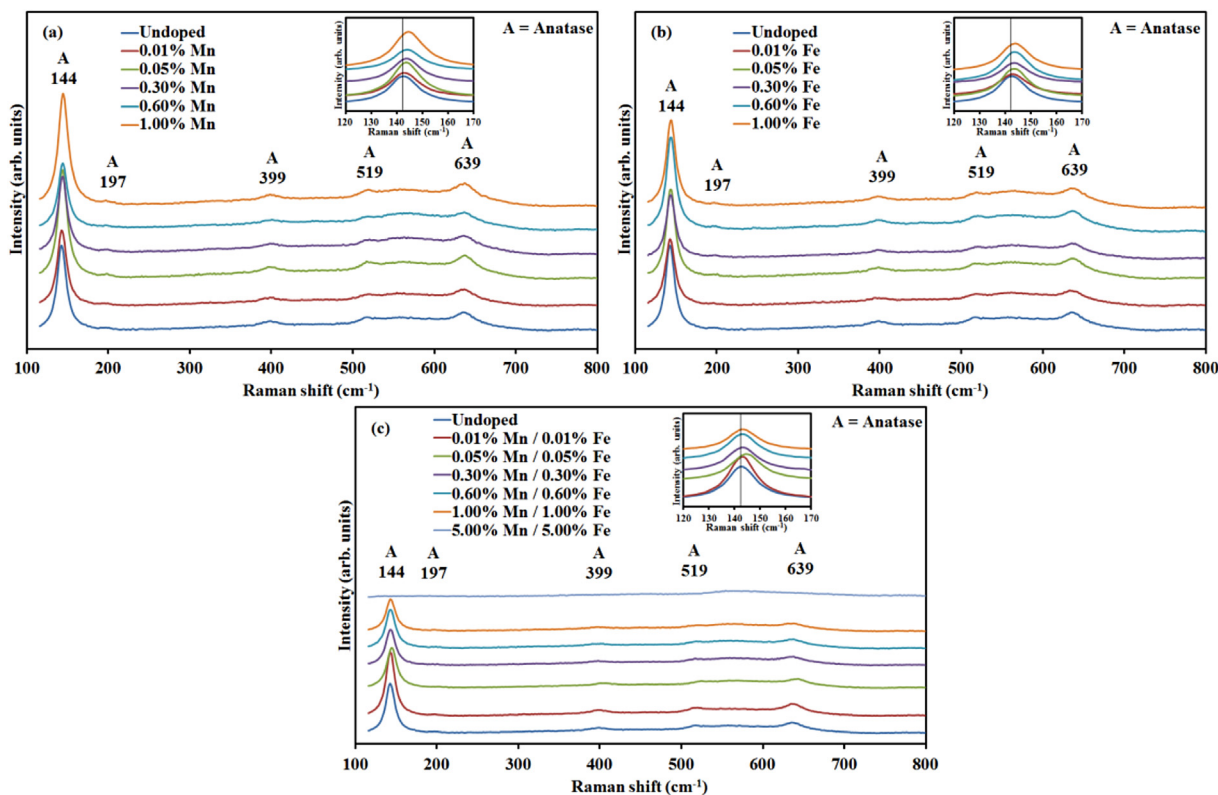


Fig. 1 – Laser Raman microspectra of TiO_2 thin films annealed at $450\text{ }^\circ\text{C}$ for 2 h at dopant levels of: (a) 0–1.00 mol% Mn, (b) 0–1.00 mol% Fe, and (c) 0/0–5.00 mol% Mn/5.00 mol% Fe codoped.

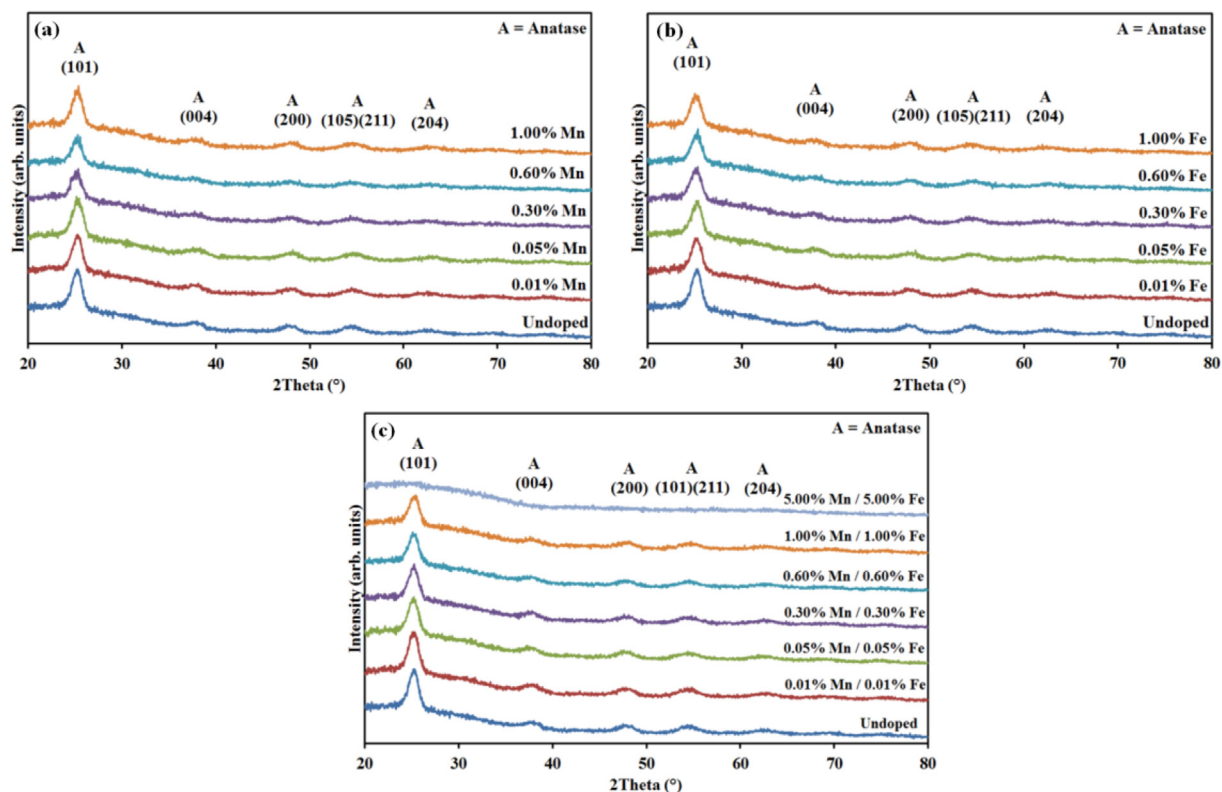


Fig. 2 – GAXRD patterns of TiO₂ thin films annealed at 450 °C for 2 h at dopant levels of: (a) 0–1.00 mol% Mn, (b) 0–1.00 mol% Fe, and (c) 0/0–5.00 mol% Mn/5.00 mol% Fe codoped.

exchange of electrons to alter the valence states, as shown in Equation (1):



This phenomenon also is expected to cause significant alteration in the oxygen vacancy concentration.

Chemical characteristics

The data for the dopant concentrations and contamination levels from the XPS analysis are shown in Table 2. Owing to the low doping concentrations, the signals of Mn and Fe could be distinguished only at doping levels ≥ 0.30 mol%. In addition, the XPS data suggest that the major contaminant in the films was Si; the concentration of Si did not change significantly with increases in the dopant concentration.

Fig. 3 shows the XPS spectra of the undoped and codoped thin films, focussing on the Mn 2p, Fe 2p, and Ti 2p peak-containing regions of the spectra. From the XPS spectra of the 0.30 mol% Mn/0.30 mol% Fe codoped sample and 1.00 mol% Mn/1.00 mol% Fe codoped sample, the Mn 2p_{3/2} peaks were located at 640.37 and 640.99 eV, respectively. The XPS spectra of these two samples showed that the Fe 2p_{3/2} peaks were located at 708.79 and 710.74 eV, respectively. The Ti 2p levels of the films showed two symmetrical doublet peaks for Ti 2p_{3/2} and Ti 2p_{1/2} located at 458.36 and 464.68 eV, respectively. It is observed that, although the peaks for Fe 2p are weak, a shift

occurred in the energy level of Fe 2p_{3/2} peak with increasing dopant concentration and this may be indicative of a change in the valence of the cation, further suggesting that intervalence charge transfer may have occurred at these concentrations [28].

Even though the presence of Mn and/or Fe ions in the samples was confirmed, the actual valences could not be determined owing to their low concentrations. Thermodynamic stability diagrams, as shown in Fig. 4 – calculated using FACTSage 6.0 (GTT Technologies, Germany) – for Mn–O and Fe–O [24], indicate that Mn³⁺ and Fe³⁺ and possibly Mn⁴⁺ (due to the proximity of the Mn³⁺/Mn⁴⁺ phase boundary) are likely to be present in the films after annealing at 450 °C in air, although Fe²⁺ could be formed by intervalence charge transfer, as indicated in Equation 1. The observed peaks representing the Ti⁴⁺ oxidation state are consistent with the thermodynamic stability diagram for Ti–O [12].

Table 2 – Data for dopant and contamination levels from XPS analysis of single-cation doped and codoped TiO₂ thin films on soda-lime-silica glass substrates.

Dopant/contaminant levels	Mn	Fe	Na	Ca	Si
Undoped	0.00	0.00	0.00	0.00	4.75
0.05 mol% Mn/0.05 mol% Fe	0.00	0.00	0.00	0.00	5.21
0.30 mol% Mn/0.30 mol% Fe	0.27	0.12	0.00	0.00	4.23
0.60 mol% Mn/0.60 mol% Fe	0.40	0.40	0.00	0.00	6.06
1.00 mol% Mn/1.00 mol% Fe	0.62	0.85	0.00	0.00	5.61

Microstructural characteristics

The morphological features of the TiO₂ thin film surfaces are shown in Fig. 5(a)–(e). The undoped and single-cation doped films (Fig. 5(a)–(c)) consisted of fairly uniformly sized grains with sizes in the range of ~20–30 nm. The addition of dopants appears to have caused agglomeration and consistent topographical alteration, although it can be seen that the measured roughness, shown by the scale bars, actually decreased with doping. This effect is confirmed by calculation of the RMS roughness, which is smaller than the scale of the particle size, as shown in Table 3. The RMS roughness data show that doping decreases the grain size in all cases of doping.

From Fig. 5(d), it can be seen that codoping causes more significant agglomeration in the 1.00 mol% Mn/1.00 mol% Fe codoped sample, with the grains within the agglomerates being <20 nm in size. For the 5.00 mol% Mn/5.00 mol% Fe codoped sample, isolated and apparently closed pores can be seen to have formed and these were rounded and bordered by relatively large grains. The grains of this sample also were <20 nm in size but these samples were amorphous, as shown in Figs. 1 and 2.

Moreover, the extent of agglomeration in the codoped samples is greater than that seen in the single-cation doped samples, where the grains comprising the former are smaller than those of the latter. This is associated with greater

structural distortion resulting from codoping, which would play a role in suppressing the nucleation of titania, thereby hindering grain growth during recrystallisation. The observation of reducing crystallinity with increasing codopant concentrations supports the conclusion that high levels (>1.00 mol % each) of codopants can hinder the recrystallisation of anatase.

At the highest codoping level of 5.00 mol% Mn/5.00 mol% Fe, there is a significant impact on the microstructure such that large apparently closed pores were observed on the film surface, which probably resulted from isolated pockets of liquid formation (based on the round appearance of the pores). The formation of liquid at these temperatures could result from the presence of high localised concentrations of the metallic species (codopants) at these regions. Since the scale of the microstructural features are ~50 nm, energy dispersive spectroscopy (EDS) cannot be used to analyse the composition as the beam has diameter of ~1000 nm.

Fig. 6 shows FEGTEM images of undoped, single-cation doped, and codoped TiO₂ thin films. The images suggest that the thickness of the films was relatively consistent at ~250 nm, irrespective of the presence or absence of dopants, the dopant type, and the dopant concentration. Further, the interface between the glass substrate and thin film showed a thin diffusion layer in the TiO₂, which is assumed to be Si contamination from the substrate, as detected by the XPS analysis and given in Table 2. All of the films indicated a general topological roughness on a coarse scale, as suggested by the AFM images of the doped samples. The absence of any variation in the thickness, despite slight variations in the grain size, is due to the fact that agglomerates tend to shrink into themselves without affecting the surrounding matrix [31]. Thus, the decrease in grain size is not significant enough to affect the film thickness.

Optical characteristics

The transmission spectra of the films are shown in Fig. 7. The results show that all of the films were highly transparent (~80%) and the only anomaly was the curve for the sample with high codopant concentrations (5.00 mol% Mn/5.00 mol% Fe). The transmission spectra showed interference fringes, which prove that the thin films are smooth and microstructurally homogenous [32]. The high transmittance of the thin films is related to the photon mean free path of light in the thin films. Light scattering from interactions with lattice defects, grain boundaries, and surfaces can affect the transmission, but, if the wavelength (400–800 nm) is greater than the grain size (≤30 nm) and film thickness (~250 nm), then light scattering is limited to the generally less significant effects of lattice defects, which thus results in a relatively high and constant transmission [33].

Tables 4 and 5 show the optical indirect band gaps (E_g) of single-cation doped and codoped thin films, respectively, and these were calculated using the Tauc equation [34]. The results show that the optical indirect band gaps of the films were quite similar to that of the undoped sample and no significant changes were observed with the addition of Mn and/or Fe as dopants. These results indicate that there is an insignificant effect of the addition of dopant on the E_g . A possible interpretation of this is that the effects of doping; the formation of

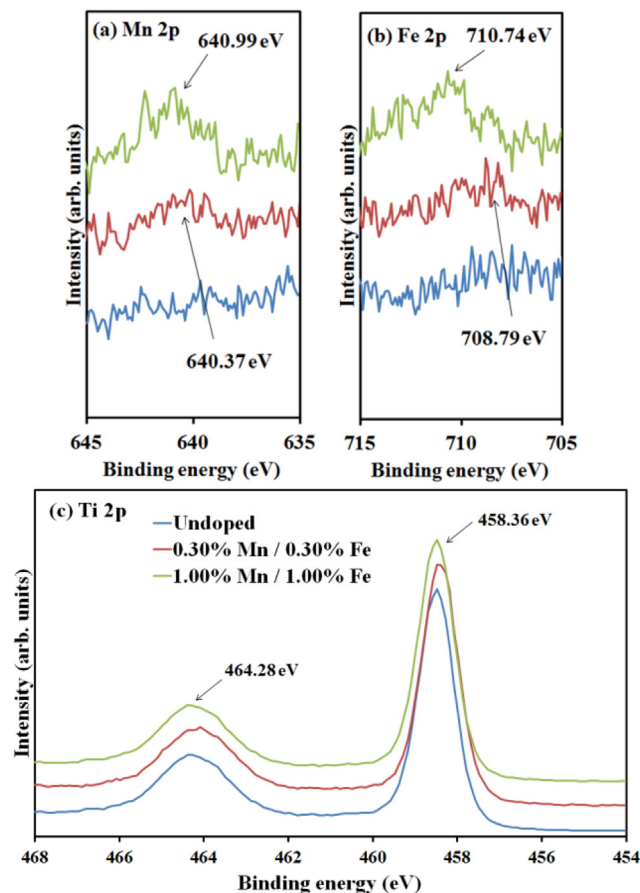


Fig. 3 – XPS peaks in undoped and codoped TiO₂ thin films representing: (a) Mn 2p, (b) Fe 2p, and (c) Ti 2p energy regions.

oxygen vacancies, which may introduce mid-gap bands to reduce the E_g oxygen vacancies [35]; lattice distortion; and other factors could negate each other [36].

Photocatalytic performance

The photocatalytic performance of the films was evaluated by the photo-bleaching of MB, as shown in Fig. 8. In comparison with the undoped TiO_2 thin film, the extent of MB solution degradation by the Mn-doped samples generally declined with increasing doping concentration; a similar trend was seen for Fe-doped samples, except in the case of 0.01 mol% Fe-doped TiO_2 thin films, which exhibited a slightly superior extent of MB solution photodegradation at the longest time point. At Fe doping levels >0.01 mol%, the photocatalytic performance of the films generally declined with increasing doping concentration. In the case of the codoped samples, it is evident that the undoped TiO_2 thin film had the best photocatalytic performance and the extent of MB solution photodegradation gradually decreased with increasing codoping levels.

Overall impact of single-cation doping and codoping on TiO_2 thin film properties and performance

There are three possibilities for the physical disposition of the dopant ions:

- (1) In the interstices
- (2) On the lattice sites
- (3) On the grain boundaries

The mineralogical analysis data indicate that the dopants enter the lattice (solid solution) rather than being located at the grain boundaries in the form of precipitates. This is because, if the dopant ions were located on the grain boundaries, they would be physically attached to the grains and no measurable impact of the vibration of molecular bonds in the TiO_2 lattice would be expected to be observed [37], i.e., no peak shift would occur. The three-dimensional representation of the TiO_6 octahedra arrangement in anatase shows that there are four edges of octahedra (with Ti^{4+}) sharing connectivity in anatase, forming one interstitial octahedron (without Ti^{4+}) [3,38]. Since the arrangement of the interstices is identical to the TiO_6 octahedra, this suggests that there would be little difference in the impact of the dopant incorporation (substitutional or interstitial) on the lattice distortion. However, the latter would require more energy owing to the more significant change in charge upon insertion of a cation. According to Hume-Rothery's rules for solid solubility in metals [39], a radius size difference of $<15\%$ allows for partial substitutional solubility, typically up to ~ 1 mol%. Based on the thermodynamic stability diagrams, it is assumed that Mn^{3+} , Mn^{4+} , and/or Fe^{3+} ions are present in the system (although Fe^{2+} is also possible due to intervalence charge transfer). Comparison of

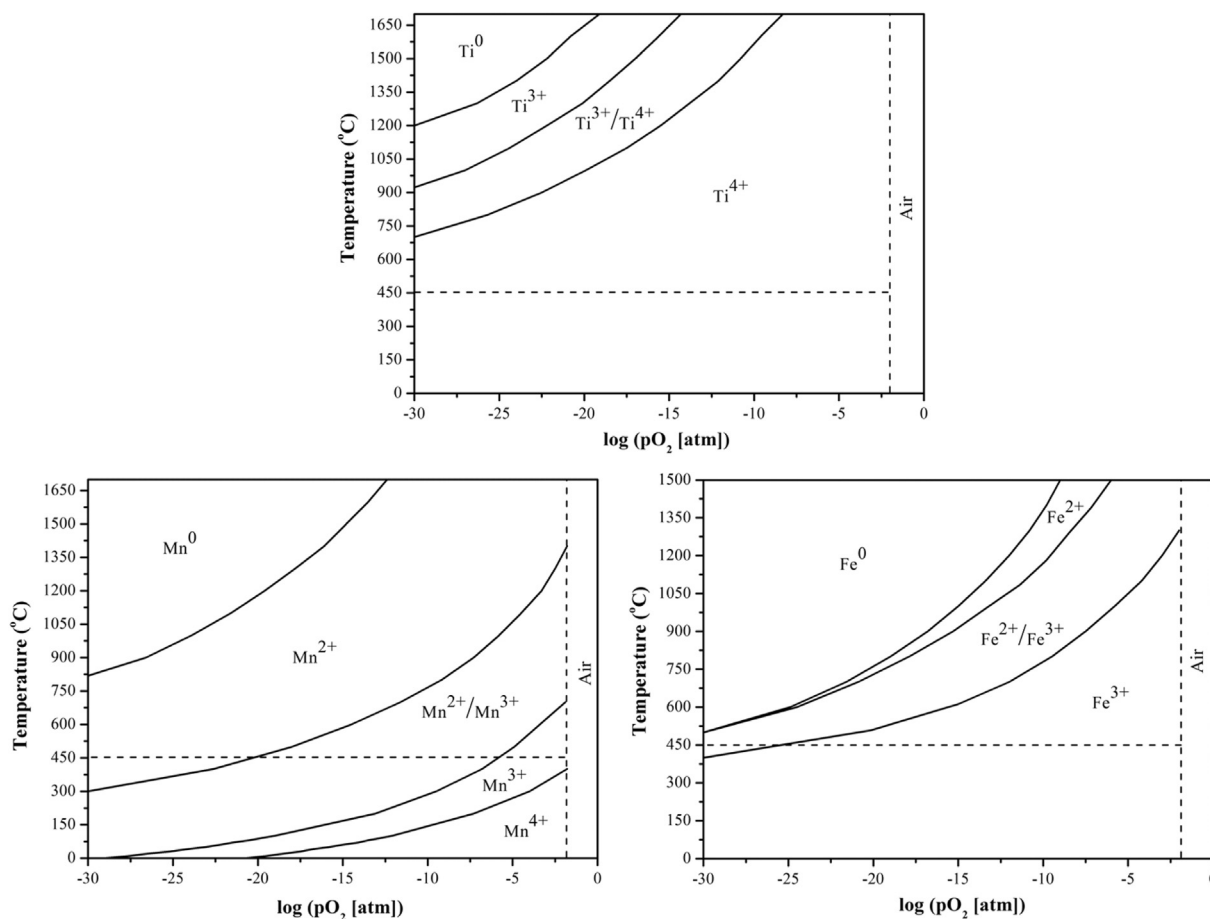


Fig. 4 – Thermodynamic stability diagrams for Ti–O, Mn–O, and Fe–O.

the crystal radii shows that all of the ions, except possibly Mn^{4+} , can form solid solutions by substitutional means and that these should cause lattice expansion.

However, the substitution of Mn^{3+} , Fe^{2+} , and/or Fe^{3+} for Ti^{4+} in the lattice also would cause the formation of oxygen vacancies in the TiO_2 lattice in order to maintain charge neutrality. Since the O^{2-} anion is much larger than the cations, its removal upon vacancy formation would cause lattice contraction, which is believed widely to be

responsible for enhancement of the photocatalytic activity, as seen in studies involving transition metal doping [3,40,41].

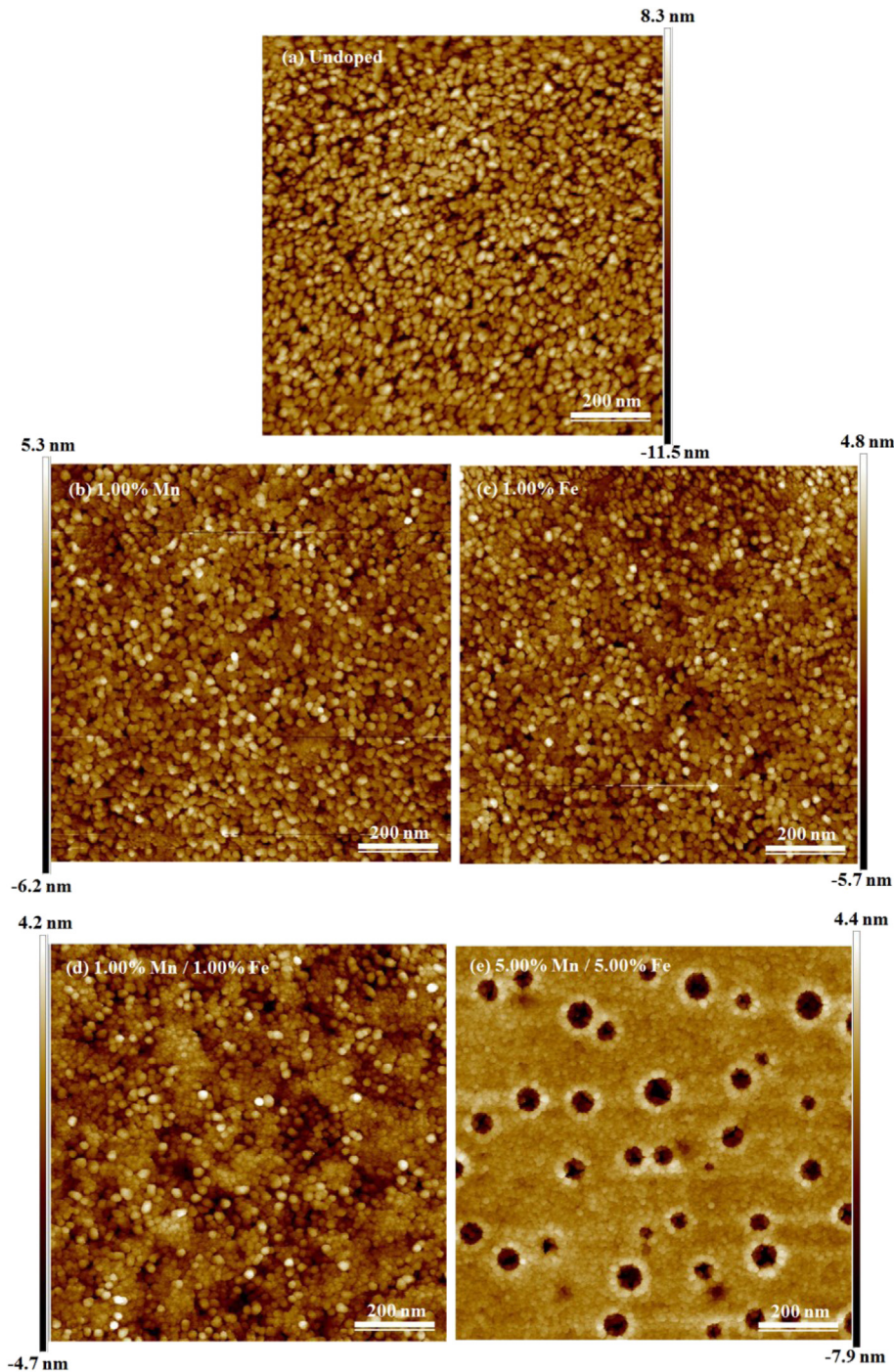


Fig. 5 – Topographical images of TiO_2 thin films annealed at $450\text{ }^\circ\text{C}$ for 2 h at dopant levels: (a) no dopants, (b) 1.00 mol% Mn, (c) 1.00 mol% Fe, (d) 1.00 mol% Fe/1.00 mol% Mn, and (e) 5.00 mol% Fe/5.00 Mn mol% codoped.

Table 3 – RMS roughness values for undoped, single-cation doped and codoped TiO₂ thin films.

Doping level		RMS roughness, R _q (nm)
Undoped		2.120
Single-cation doped (mol%)	1.00 Mn	1.100
	1.00 Fe	1.040
Codoped (mol%)	0.05/0.05	1.810
Mn/mol% Fe)	0.30/0.30	1.320
	0.60/0.60	0.985
	1.00/1.00	0.877
	5.00/5.00	0.814

Equations 2–4 show that the substitution of Fe²⁺ would create more oxygen vacancies and this would be expected to result in a higher extent of lattice contraction compared to the cases of Mn³⁺ or Fe³⁺ ions. This observation suggests the advantage of reduction firing of Fe-doped TiO₂.

If doping occurs at a substitutional position on the Ti⁴⁺ site, the Ti–O–Ti bond will be removed due to the formation of an M–O–Ti or M–O–M bond (M denotes Mn or Fe) and this would result in an oxygen vacancy since the valence of the dopant ions is lower than that of Ti. Hence, the removal of the Ti–O–Ti bond and the formation of new M–O bonds would

cause a shift in the Raman peaks, although the observed shift could be the result of oxygen vacancies as well.

The photocatalytic performance of the thin films is affected by two competing factors:

- Lower band gap levels (and other semiconducting properties, which are unknown) created by doping ions are expected to have a positive effect on the performance [13,16].
- Lattice distortion, which is expected to have a negative effect on the performance at high doping concentrations [33].

In a more general consideration of the issue, for Mn³⁺, the crystal radius (0.0785 nm) is similar to that of Ti⁴⁺ (0.0745 nm) but there is a valence difference between the dopants, which leads to oxygen vacancy formation upon substitution. For Mn⁴⁺, the crystal radius is smaller (0.0670 nm) than that of Ti⁴⁺ but there is no valence difference between cations. Hence, while both Mn³⁺ and Mn⁴⁺ could cause lattice contraction when substituted for Ti⁴⁺, only Mn³⁺ would alter the anion defect state. On the other hand, if Mn³⁺ or Mn⁴⁺ formed interstitial solid solutions, facilitated by the equivalence of sizes of the octahedral interstices and the Ti in filled octahedra, the situation would be different and therefore, in order to maintain charge neutrality, oxygen injection would be required and this would cause lattice expansion. Oxidation

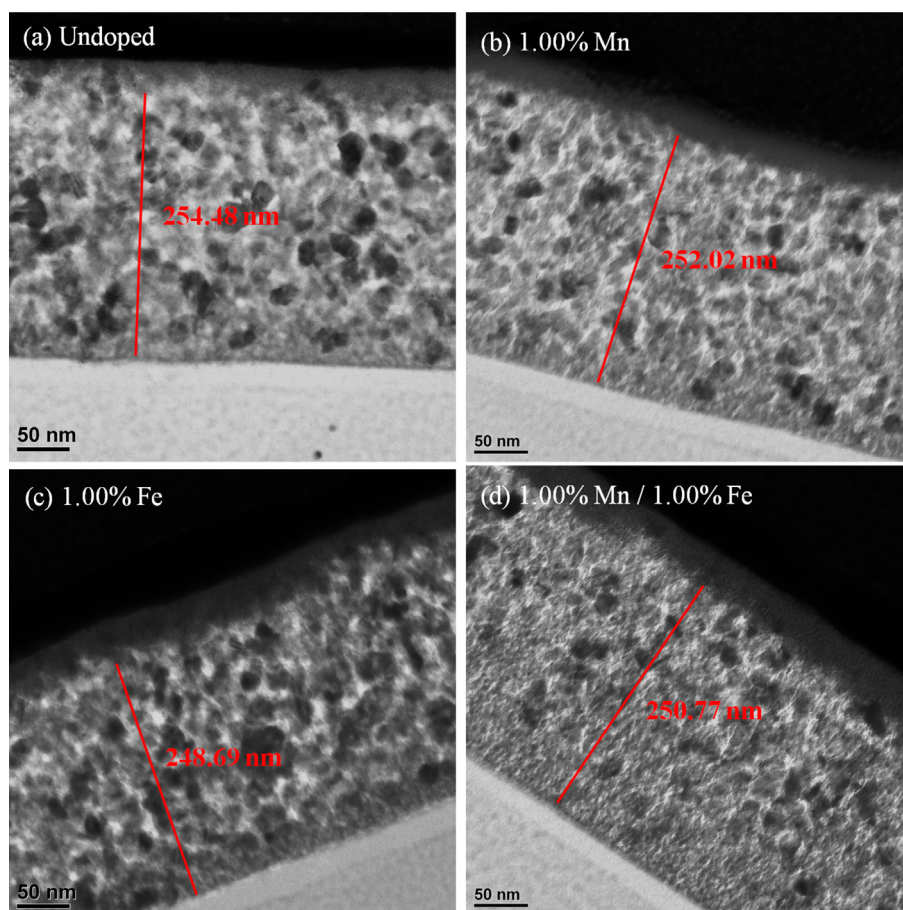


Fig. 6 – FEGTEM cross-sectional images of TiO₂ thin films annealed at 450 °C for 2 h at dopant levels of: (a) undoped, (b) 1 mol % Mn doped, (c) 1 mol% Fe doped, and (d) 1.00 mol% Mn/1.00 Fe mol% codoped.

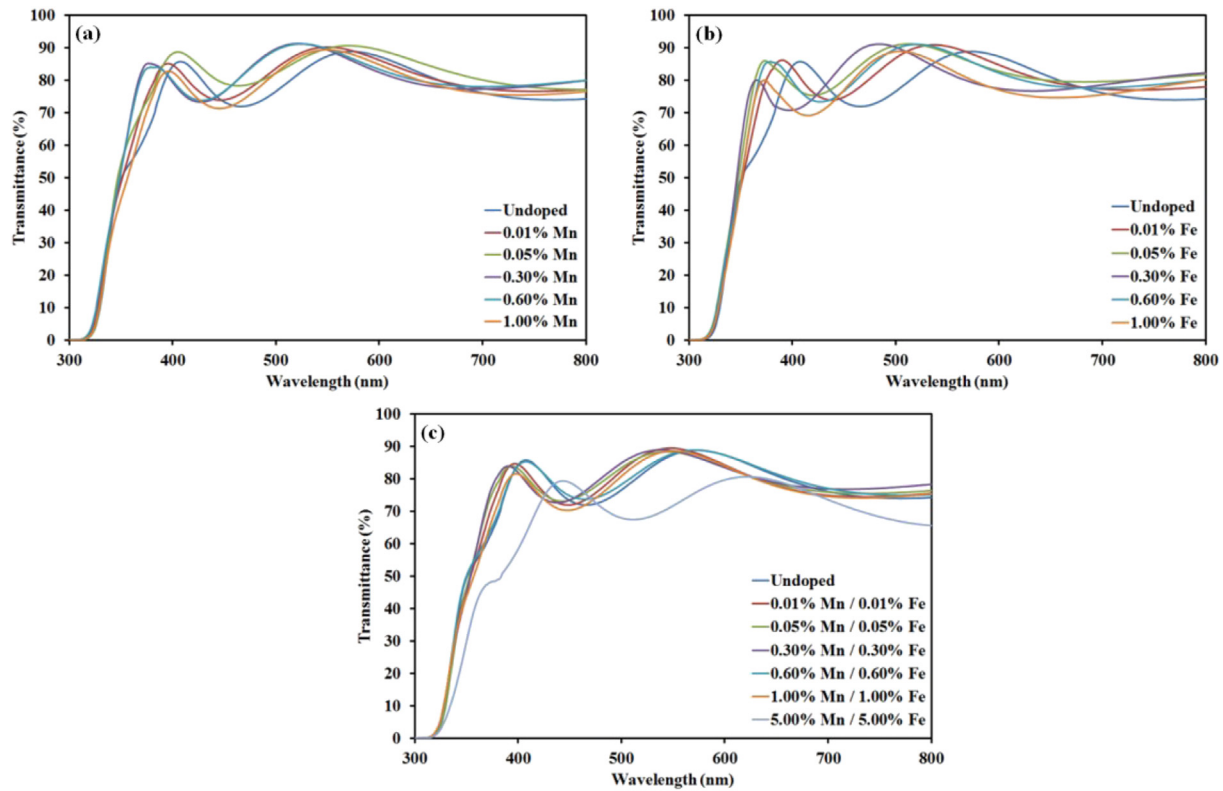


Fig. 7 – UV–VIS transmission spectra of TiO_2 thin films annealed at 450°C for 2 h at dopant levels of: (a) 0–1.00 mol% Mn, (b) 0–1.00 mol% Fe, and (c) 0–5.00 mol% Mn/0–5.00 mol% Fe codoped.

is possible owing to the real stoichiometry of titania being TiO_{2-x} and not TiO_2 [26].

In the case of Fe-doped samples, the crystal radii of both Fe^{2+} (0.0780 nm) and Fe^{3+} (0.0785 nm) are similar to that of Ti^{4+} (0.0745 nm) but there are valence differences between Fe^{2+} and Fe^{3+} in comparison with Ti^{4+} . These ions also would cause lattice contraction in the case of substitution of Fe^{2+} and Fe^{3+} for Ti^{4+} . However, if Fe^{2+} or Fe^{3+} formed interstitial solid solutions, this could cause lattice expansion owing to the necessity for oxidation. Thus, the photocatalytic efficiency would be affected by the role of the doping ions in either serving as mediators for interfacial charge transfer or acting as recombination centres [41,42]. If doping ions act as electron and/or hole traps at the donor and acceptor levels, they could impede electron–hole recombination and enhance interfacial charge transfer, thus facilitating decomposition of the organics adsorbed on the surface of TiO_2 . However, when the dopant concentration is too high, the recombination rates would increase because the distance between the trapping sites decreases with the number of dopant ions.

Based on the above discussion, it is clear that the lattice distortion decreases the crystallinity of the films (especially for 5.00 mol% Mn/5.00 mol% Fe, which is amorphous) and the photocatalytic performance probably degrades owing to this distortion. This is in agreement with the work of others, who investigated the effect of doping on lattice distortion [33,41]. Moreover, at the higher dopant levels, the photocatalytic efficiency of crystalline TiO_2 would decrease due to the increase in the recombination rates. Thus, the films were observed generally to show decreasing performance with increasing dopant concentration. However, in the case of 0.01 mol% Fe-doped sample, the data suggest that there may be an increase in photocatalytic performance at this lowest dopant level (at the longest time point), which indicates that most samples probably were overdoped since a small amount of doping ions (0.01 mol%) may act as recombination centres but the very minor lattice distortion is not sufficient to decrease the photoactivity. Thus, it is possible that doping with Mn^{3+} or Mn^{4+} ions and in codoped films may be more effective at levels of $<0.01\%$.

Table 4 – Optical indirect band gaps of TiO_2 thin films annealed at 450°C for 2 h containing varying single-cation dopant (Mn or Fe) concentrations.

Optical indirect band gap (eV)	Undoped	0.01 mol%	0.05 mol%	0.30 mol%	0.60 mol%	1.00 mol%
Mn doping	3.43	3.46	3.44	3.47	3.48	3.45
Fe doping		3.45	3.47	3.45	3.46	3.45

Table 5 – Optical indirect band gaps of TiO₂ thin films annealed at 450 °C for 2 h containing varying codopant (Mn and Fe) concentrations.

Mn (mol%)	Undoped	0.01	0.05	0.30	0.60	1.00	5.00
Fe (mol%)		0.01	0.05	0.30	0.60	1.00	5.00
Optical indirect band gap (eV)	3.43	3.45	3.42	3.46	3.45	3.46	3.39

Conclusions

The major conclusions from the present work are as follows:

- Mineralogical analysis showed that the films contain pure anatase (only 5.00 mol% Mn/5.00 mol% Fe sample is amorphous), suggesting that Mn and Fe ions are incorporated in the TiO₂ lattice to form solid solutions.
- Microstructural analysis shows that the surfaces of the films are highly uniform and most of the films contain grains in the size range ~20–30 nm. The thickness of the films is ~250 nm. The addition of dopants suppresses grain growth and enhances agglomeration and roughening of the films. These are attributed to the effect of the dopants in hindering the recrystallisation of titania and subsequent grain growth. At the highest codoping level of 5.00 mol% Mn/5.00 mol% Fe, large apparently closed pores, probably resulting from liquid formation, were observed on the film surface and these were attributed to localized concentrations of the codopants.

- XPS analysis and thermodynamic stability diagrams indicate that Ti⁴⁺, Mn³⁺, Fe³⁺, and possibly Mn⁴⁺ are likely to be incorporated in the films after annealing at 450 °C for 2 h in air. In the codoped films, Fe²⁺ may be present in the films due to intervalence charge transfer. Mn³⁺, Fe²⁺, and/or Fe³⁺ ions can form substitutional solid solutions. The substitution of Mn³⁺, Fe²⁺, and/or Fe³⁺ for Ti⁴⁺ results in oxygen vacancy formation and this would cause lattice contraction. The additional need for oxygen in the case of interstitial doping to maintain electrical neutrality would be expected to cause lattice expansion.
- UV–VIS transmission spectrophotometry data show that the films are highly transparent (~80%) and that the E_g remains relatively unchanged with increasing doping levels. The only anomaly is the sample containing 5.00 mol% Mn/5.00 mol% Fe, which is believed to result from the effects of increased porosity and the amorphous nature of the film.
- Photocatalytic testing shows that the extent of photo-degradation diminishes with increasing dopant concentration. Only the 0.01 mol% Fe-doped TiO₂ film shows superior photoactivity (at the longest time point). The low amount of dopant minimises the number of recombination centres, which would assist photoactivity, but the lattice distortion, which would hinder photoactivity, also is minimised

It is probable that consideration of these two effects will be important in the potential use of dopants to improve the band gap without degrading the performance by increasing the

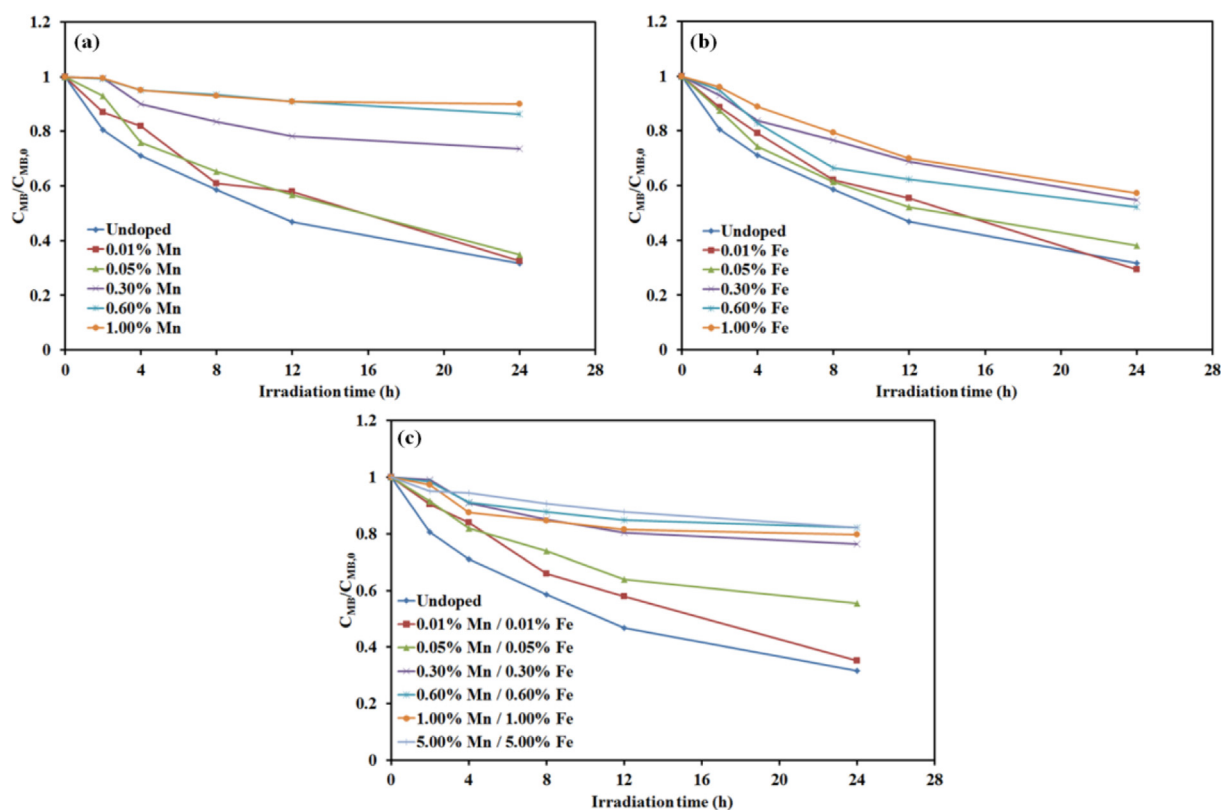


Fig. 8 – Degradation curves of MB solution at different irradiation times photocatalysed by different TiO₂ films containing varying amounts of single-cation dopants and codopants.

number of recombination centres and enhancing lattice distortion.

Acknowledgements

The authors are grateful for the financial support of the Australian Research Council (ARC), which has allowed for this and other related developmental work to be undertaken. The authors also would like to acknowledge the UNSW node of the Australian Microscopy & Microanalysis Research Facility (AMMRF) for the use of their facilities for the analytical work.

REFERENCES

- [1] Ismail AA, Bouzid H. Synthesis of mesoporous ceria/titania thin films for self-cleaning applications. *J Colloid Interf Sci* 2013;404:127–34.
- [2] O'Regan B, Gratzel M. A low-cost, high-efficiency solar cell based on dye-sensitized colloidal TiO₂ films. *Nature* 1991;353:737–40.
- [3] Hanaor D, Sorrell C. Review of the anatase to rutile phase transformation. *J Mater Sci* 2011;46:855–74.
- [4] Wu K-R, Hung C-H. Characterization of N,C-codoped TiO₂ films prepared by reactive DC magnetron sputtering. *Appl Surf Sci* 2009;256:1595–603.
- [5] Wang SJ, Chang WT, Ciou JY, Wei MK, Wong MS. Preparation of TiO₂ thin films by laser ablation for photocatalytic applications. 4 ed. Seattle, Washington (USA): AVS; 2008. pp. 898–902.
- [6] Yang H, Zhang X, Tao Q. Synthesis and characterization of Sol–Gel derived TiO₂ thin films: effect of different pretreatment process. *Inorg Mater* 2009;45:1139–45.
- [7] Tsoukleris DS, Kontos AI, Aloupogiannis P, Falaras P. Photocatalytic properties of screen-printed titania. *Catal Today* 2007;124:110–7.
- [8] Sokolov S, Ortel E, Radnik J, Kraehnert R. Influence of steel composition and pre-treatment conditions on morphology and microstructure of TiO₂ mesoporous layers produced by dip coating on steel substrates. *Thin Solid Films* 2009;518:27–35.
- [9] Oja Acik I, Junolainen A, Mikli V, Danilson M, Krunks M. Growth of ultra-thin TiO₂ films by spray pyrolysis on different substrates. *Appl Surf Sci* 2009;256:1391–494.
- [10] Wang MC, Lin HJ, Yang TS. Characteristics and optical properties of iron ion (Fe³⁺)-doped titanium oxide thin films prepared by a sol–gel spin coating. *J Alloys Compd* 2009;473:394–400.
- [11] Nakaruk A, Lin C, Perera D, Sorrell C. Effect of annealing temperature on titania thin films prepared by spin coating. *J Sol–Gel Sci Tech* 2010;55:328–34.
- [12] Fuyuki T, Matsunami H. Electronic properties of the interface between Si and TiO₂ deposited at very low temperatures. *Jpn J Appl Phys* 1986;25:1288–91.
- [13] Deng QR, Xia XH, Guo ML, Gao Y, Shao G. Mn-doped TiO₂ nanopowders with remarkable visible light photocatalytic activity. *Mater Lett* 2011;65:2051–4.
- [14] Zaleska A. Doped-TiO₂: a review. *Recent Patents Eng* 2008;2:157–64.
- [15] Naeem K, Ouyang F. Preparation of Fe³⁺-doped TiO₂ nanoparticles and its photocatalytic activity under UV light. *Physica B* 2010;405:221–6.
- [16] Wu JCS, Chen C-H. A visible-light response vanadium-doped titania nanocatalyst by sol–gel method. *J Photochem* 2004;163:509–15.
- [17] Devi LG, Murthy BN. Characterization of Mo doped TiO₂ and its enhanced photo catalytic activity under visible light. *Catal Lett* 2008;125:320–30.
- [18] Jia L, Wu C, Han S, Yao N, Li Y, Li Z, et al. Theoretical study on the electronic and optical properties of (N, Fe)-codoped anatase TiO₂ photocatalyst. *J Alloys Compd* 2011;509:6067–71.
- [19] Hu Y, Zhang X, Wei C. Synthesis of Mn-N-codoped TiO₂ photocatalyst and its photocatalytic reactivity under visible light irradiation. *Mater Sci Forum* 2009;620–622:683–6.
- [20] Estrellan CR, Salim C, Hinode H. Photocatalytic activity of sol–gel derived TiO₂ co-doped with iron and niobium. *React Kinet Catal Lett* 2009;98:187–92.
- [21] Guo J, Gab Z, Lu Z, Liu J, Xi J, Wan Y, et al. Improvement of the photocatalytic properties of TiO₂ by (Fe+Mo) co-doping – A possible way to retard the recombination process. *J Appl Phys* 2013;114:1–7. 104903.
- [22] Shi Z, Lai H, Yao S, Wang S. Photocatalytic activity of Fe and Ce co-doped mesoporous TiO₂ catalyst under UV and visible light. *J Chin Chem Soc* 2012;59:614–20.
- [23] Sun T, Fan J, Liu E, Liu L, Wang Y, Dai H, et al. Fe and Ni co-doped TiO₂ nanoparticles prepared by alcohol-thermal method: Application in hydrogen evolution by water splitting under visible light irradiation. *Powd Tech* 2012;228:210–8.
- [24] Nakaruk A, Lin CYW, Chaneei D, Koshy P, Sorrell CC. Fe-doped and Mn-doped titanium dioxide thin films. *J Sol–Gel Sci Technol* 2012;61:175–8.
- [25] Mills A, McFarlane M. Current and possible future methods of assessing the activities of photocatalyst films. *Catal Today* 2007;129:22–8.
- [26] Nowotny J, Bak T, Nowotny MK, Sheppard LR. Titanium dioxide for solar-hydrogen II. Defect chemistry. *Int J Hydrogen Energy* 2007;32:2630–43.
- [27] Shannon RD, Prewitt CT. Effective ionic radii in oxides and fluorides. *Acta Crystallogr B* 1969;25:925–46.
- [28] Hu S, Li F, Fan Z, Chang C-C. Enhanced photocatalytic activity and stability of nano-scaled TiO₂ co-doped with N and Fe. *Appl Surf Sci* 2011;258:182–8.
- [29] Li X, Chen Z, Shi Y, Liu Y. Preparation of N, Fe co-doped TiO₂ with visible light response. *Powder Technol* 2011;207:165–9.
- [30] Nassau K. The physics and chemistry of color. In: The fifteen causes of color. 2nd ed. New York: Wiley; 1983.
- [31] Kingery W, Bowen H, Uhlmann D. Introduction to ceramics. 2 ed. New York: Wiley; 1976.
- [32] Swanepoel R. Determination of surface roughness and optical constants of inhomogeneous amorphous silicon films. *J Phys E Sci Instrum* 1984;17:896.
- [33] Jing LQ, Sun ZH, Wang BQ, Qu YC, Fu HG. Preparation and characterization of La doped TiO₂ nanoparticles by sol-hydrothermal method. *J Inorg Mater* 2005;20:789–93.
- [34] Mardare D, Tasca M, Delibas M, Rusu GI. On the structural properties and optical transmittance of TiO₂ r.f. sputtered thin films. *Appl Surf Sci* 2000;156:200–6.
- [35] Nakaruk A, Ragazzon D, Sorrell CC. Anatase thin films by ultrasonic spray pyrolysis. *J Anal Appl Pyrol* 2010;88:98–101.
- [36] Nakaruk A, Ragazzon D, Sorrell CC. Anatase–rutile transformation through high-temperature annealing of titania films produced by ultrasonic spray pyrolysis. *Thin Solid Films* 2010;518:3735–42.
- [37] Tian F, Zhang Y, Zhang J, Pan C. Raman spectroscopy: a new approach to measure the percentage of anatase TiO₂ exposed (001) facets. *J Phys Chem C* 2012;116:7515–9.
- [38] Bokhimi X, Morales A, Aguilar M, Toledo-Antonio JA, Pedraza F. Local order in titania polymorphs. *Int J Hydrogen Energy* 2001;26:1279–87.
- [39] Hume-Rothery W, Smallman RE, Haworth CW. Structure of metals and alloys; 1969. Belgrave Square London.

-
- [40] Gan J, Lu X, Wu J, Xie S, Zhai T, Yu M, et al. Oxygen vacancies promoting photoelectrochemical performance of In_2O_3 nanocubes. *Sci Rep* 2013;3.
- [41] Akpan UG, Hameed BH. The advancements in sol–gel method of doped- TiO_2 photocatalysts. *Appl Catal* 2010;375:1–11.
- [42] Choi W, Termin A, Hoffmann MR. The role of metal ion dopants in quantum-sized TiO_2 : correlation between photoreactivity and charge carrier recombination dynamics. *J Phys Chem* 1994;98:13669–79.